LAWRENCE
LIVERMORE
NATIONAL
LABORATORY

LLNL-TR-763703

Analysis of Three-Component Rotational and Translational Ground Motions from Source Physics Experiment Chemical Explosions and Local Earthquakes

G. A. Ichinose, S. R. Ford, R. Mellors

December 6, 2018

Disclaimer

This document was prepared as an account of work sponsored by an agency of the United States government. Neither the United States government nor Lawrence Livermore National Security, LLC, nor any of their employees makes any warranty, expressed or implied, or assumes any legal liability or responsibility for the accuracy, completeness, or usefulness of any information, apparatus, product, or process disclosed, or represents that its use would not infringe privately owned rights. Reference herein to any specific commercial product, process, or service by trade name, trademark, manufacturer, or otherwise does not necessarily constitute or imply its endorsement, recommendation, or favoring by the United States government or Lawrence Livermore National Security, LLC. The views and opinions of authors expressed herein do not necessarily state or reflect those of the United States government or Lawrence Livermore National Security, LLC, and shall not be used for advertising or product endorsement purposes.

This work performed under the auspices of the U.S. Department of Energy by Lawrence Livermore National Laboratory under Contract DE-AC52-07NA27344.

Analysis of Three-Component Rotational and Translational Ground Motions from Source Physics Experiment Chemical Explosions and Local Earthquakes

Gene A. Ichinose, Sean Ford, and Robert Mellors

Abstract

Igel et al. (2005) demonstrated that using single point measurements of translational displacement and rotational strain can reconstruct the long-period teleseismic wavefield including wave-type, apparent velocity and propagation direction. We examine if this also holds true for higher frequencies at local distances. Four co-located three-component (3C) Eentec R-1 rotational velocity sensors and Kinemetric 3C accelerometers were deployed at the Nevada National Security Site (NNSS) to record 3 Source Physics Experiment (SPE) chemical explosions with yields of 90kg (SPE-1), 997kg (SPE-2), and 905kg (SPE-3) equivalent TNT. The four sensors were deployed 1-km from the source on granite, sedimentary, and alluvium outcrops. Three small earthquakes were also recorded, a Ml 3.3 at 28 km, a Ml 2.6 at 58 km, and Ml 3.5 at 123 km distance from SPE site. From the 3C rotational and translational motions, we measured the horizontal phase velocity of 450 m/s and 1125 m/s along two separate directions from the source consistent with near-surface geology. In contrast, the horizontal phase velocity measured for the Ml 3.3 earthquake is 5.4 km/s in the 0.1 to 10 Hz band with a propagation direction consistent with the epicenter location. While the earthquake exhibited very high coherency between 3C rotational and translational motions, the explosions exhibited more coherency with P-SV waves but less for SH-waves. This may be due to explosion SH-waves originating from motions along joints or scattering near the source. This difference could be exploited as a discriminant between explosions and earthquakes.

Introduction

Dense seismic arrays of three-component (3C) sensors measure particle motion to determine wavefield characteristics, propagation direction and apparent velocities. These sensors measure the wavefield but not its spatial derivatives that can be approximated from differences between individual sensors. *Igel et al.* (2005) and *Aldridge and Abbott* (2009) demonstrated that a co-located point measurement of both particle velocity and rotation using 3C seismometers and 3C rotational sensors can measure the full wavefield and spatial gradients proving that a 6C seismic sensor would be the most useful to seismologists.

Elastic theory states that 12-degrees of freedom is necessary to fully characterize motion from elastic deformation: 3 translational, 6 strain and 3 rotational components. The bulk of seismology is built upon the observations of only 3-translational components. We will show that with the assumption of plane wave propagation we can estimate the phase velocity and direction of propagation just from the 3-translational and 3-rotational components.

The main goal of our study is to see if explosion sources generate rotational motions and will they agree with classical elastic theory. *Igel et al.* (2005) and *Lin et al.* (2011) initially showed long-period rotational motions induced by large teleseismic earthquakes were consistent with classical elastic theory by comparison of point rotational measurements from ring lasers or 3C electrochemical sensors and 3C translational sensors (broadband or accelerometers). Previous work by *Nigbor* (1994), *Lin et al.* (2009) and *Langston et al.* (2009) observe rotational motions from Non-Proliferation Experiment (NPE) and Taiwan Integrated Geodynamics Research (TAIGER) chemical explosions but do not provide direct comparisons of rotational

with translational seismic data. We have 3C rotational and translational sensor data for point measurements. Point observations of rotational ground motions are beneficial compared to array derived from translational sensors because the estimated rotational motions are averaged across an array where there is potentially a loss of spatial resolution.

The explosion and earthquake data in this study will provide comparison with much higher frequency body waves (1-20 Hz) rather than longer period surface waves. We will also show whether spherical or plane wave assumption will hold because our sensors are only 1-km from the source. Pure isotropic sources should not generate rotational P- or S-waves, however we expect the free-surface, scattering and any other source asymmetries to cause rotational motions at 1 km distance. We expect rotational motions will travel with shear-waves not compressional-waves.

Data

Three-component Eentic R1 rotational velocity sensors were deployed for a time period spanning the execution of SPE-1, SPE-2 and SPE-3 chemical explosions between 03-May-2011 and 24-July-2012. The rotational sensors were co-located with Kinemetric 3-C Episensor accelerometers. Episensor (FBA ES-T) channel sensitivity was 4.1943E+05 (cnts/V) and 1.25 (V/g). Instrument response was not corrected, we scaled the amplitudes to true ground motion units of acceleration (mm/(sec*sec)). We performed a test using the full instrument response correction, but it only made an insignificant 2% difference in waveform shape above 1 Hz between the corrected waveform and original gain scaled waveform. Eentic R1 rotational velocity sensors sensitivity is 6.7275E+06 (rad/sec)/V. Instrument response was not corrected, we again scaled amplitudes to true units of rotational velocity (rad/sec). Both rotational and acceleration responses were flat between 0.01-250 Hz (sampling rate Nyquist frequency). Most of the spectral energy in the data was between 10-30 Hz. Figure 1 shows the location of Eentic R1 and Episenor sensors in relation of the source location at borehole U-15n. Stations were located along 4 lines oriented north, northeast, south, and west directions at 1 km distance from shot borehole U-15n. Stations along line 1 (L1-10) and line 5 (L5-10) recorded all three SPE shots. There was no rotational data for station L3-10 on SPE-1 and station L2-10 for SPE-1 and SPE-2, however the station L3-10 did record one of the earthquakes on 15-June-2012. For the rest of the SPE shots the stations L3-10 and L2-10 were unusable because of high noise or baseline drift with the rotational and accelerometer sensors.

We compared the waveforms between SPE events as a consistency test. SPE-2 and SPE-3 events were located in borehole U-15n with similar chemical yields and emplacement depths, therefore we expect similar shape waveforms. The SPE-1 shot size was a factor of 10 smaller, therefore we convolved it with an arbitrary triangle source-time function to make the waveforms recorded have the same frequency content as the larger shots. Figure 2 shows the station L1-10 accelerations for the vertical, radial and transverse components (CNZ, CNR, CNT) for each of the SPE shots 1-3. Figure 3 shows 3C rotational motions (DJZ, DJR, DJT) similar to Figure 2. The rotational rates were consistent between the 3 SPE shots as expected demonstrating no issues with sensor orientation errors. We did notice an inconsistency with the accelerometer components CNZ and CNT during SPE-3 event for station L1-10. We swapped those channels for the analysis of the SPE-3 and two earthquakes during the time-frame of summer 2012. We did the consistency check with station L5-10 shown in Figures 4 and 5. We also found the same inconsistency with the accelerometer components CNZ and CNT during the SPE-3 time-frame and swapped the channels in the analysis.

Methods

In classical elastic theory, the vector displacement $\boldsymbol{u}(\mathbf{x})$ at vector position $\boldsymbol{x} = (x, y, z)$ and displacement at a neighboring point $\boldsymbol{u}(\boldsymbol{x} + \delta\boldsymbol{x})$, assuming infinitesimal deformations, can be written as (Equation 1),

$$\boldsymbol{u}(\boldsymbol{x} + \delta\boldsymbol{x}) = \boldsymbol{u}(\boldsymbol{x}) + (\delta\boldsymbol{x} \cdot \nabla)\, \boldsymbol{u}$$
$$\boldsymbol{u}(\boldsymbol{x} + \delta\boldsymbol{x}) = \boldsymbol{u}(x) + \boldsymbol{\varepsilon}\, \delta\boldsymbol{x} + \boldsymbol{\Omega}\, \delta\boldsymbol{x}$$
$$\boldsymbol{u}(\boldsymbol{x} + \delta\boldsymbol{x}) = \boldsymbol{u}(x) + \boldsymbol{\varepsilon}\, \delta\boldsymbol{x} + \boldsymbol{\omega} \times \delta\boldsymbol{x}$$

where $\boldsymbol{\varepsilon}$ is the symmetric strain tensor with 6 independent elements, and $\boldsymbol{\Omega}$ is the antisymmetric rigid body rotation tensor. This rotation tensor has 3 independent vector components and often written as rotation vector $\boldsymbol{\omega}$ (Equation 2),

$$\boldsymbol{\omega} = \frac{1}{2} \nabla \times u(\boldsymbol{x})$$

$$\omega_x = \tfrac{1}{2}\left(\frac{\partial u_z}{\partial y} - \frac{\partial u_y}{\partial z}\right),\ \omega_y = \tfrac{1}{2}\left(\frac{\partial u_x}{\partial z} - \frac{\partial u_z}{\partial x}\right),\ \omega_z = \tfrac{1}{2}\left(\frac{\partial u_y}{\partial x} - \frac{\partial u_x}{\partial y}\right).$$

The above derivation underlies the importance of recording not just the 3 components of displacement $\boldsymbol{u}$ but also the 6 components of strain $\boldsymbol{\varepsilon}$ and 3 components of rotation $\boldsymbol{\omega}$ in the study of seismic deformation. We can still extract additional information about the propagating wave including the phase velocity and direction of propagation with co-located 3C displacement and rotations. In the comparisons between rotations and translations we consider the case of vector plane wave $\boldsymbol{u}(x, y, z, t) = (0, u_y\left(t - \frac{x}{c}\right), 0)$ traveling down the *x*-direction polarized in the *y*-direction with a horizontal component of the phase velocity *c*. The vector of rotation is thus given as $\frac{1}{2}\nabla \times \boldsymbol{u} = (0, 0, -\frac{1}{2c}\dot{u}_y\left(t - \frac{x}{c}\right))$ with the corresponding *z*-component of rotation rate $\dot{\omega}_z$ in the horizontal *x*-*y* plane about the *z*-axes given as (Equation 3)

$$\dot{\omega}_z = -\frac{1}{2c}\ddot{u}_y\left(t - \frac{x}{c}\right) \ \ or \ \ \frac{\ddot{u}_y}{\dot{\omega}_z} = -2c.$$

This implies that under the given assumptions the ratio of the transverse acceleration $\ddot{u}_y$ and rotation rate $\dot{\omega}_z$ should be in phase and scaled by a factor of -2*c* in amplitude. This method was successfully applied by *Igel et al.* (2005) using teleseismic long-period Love-waves recorded by broadband seismometer and ring-laser at Wettzell, Germany to make point estimates of the phase velocity and wave propagation back-azimuth. Lin et al. (2011) subsequently demonstrated the application with a 3C rotational seismometer instead of a ring-laser on surface-waves. Given the free-surface conditions, the ratio of the accelerations $\ddot{u}_x$ and $\ddot{u}_z$ with the rotation rate of the other two components $\dot{\omega}_x$ and $\dot{\omega}_y$ also leads to estimates of the other components of the phase velocity vector $\boldsymbol{c}$ but without the factor of -1/2 (*e.g., Cochard et al.*, 2006; *Lin et al.,* 2011).

Beamforming using vertical rotation rate and transverse acceleration involves rotating the horizontal acceleration components and scaling the amplitudes for finding the maximum cross-correlation and lowest amplitude misfit to solve for best fitting phase velocity and wave

propagation back-azimuth. This can be applied to a sliding time window in an appropriate frequency band (*e.g., Igel et al.*, 2006).

Results

For the comparisons shown in Figures 6 and 7 we align the appropriate components between rotational and accelerometer waveform data in absolute time. The horizontal component accelerometer and rotational sensors were installed oriented in the source-receiver (*i.e.*, radial and transverse) coordinate system instead of the geodetic (*i.e.*, north-south and east-west) coordinate system. With the plane wave assumption (see Equation 3), we expect the horizontal rotation rate in the *x*-*y* horizontal plane about the vertical *z*-axes (*i.e.*, the component DJZ) to be in phase with the transverse component acceleration CNT. In similar derivation, we expect the radial rotational component DJR about the radial axes to be in phase with the vertical component acceleration CNZ. The same for the transverse rotational component DJT about the transverse axes and the radial component acceleration CNR. Since the radial and vertical component accelerations (CNR and CNZ) contain polarized P- and SV-waves, then we expect rotational components DJT and DJR to be associated with SV- and converted P-to-SV-waves. The accelerometer component CNT contains polarized SH-waves and therefore the rotational component DJZ should also be associated with SH-waves.

We estimated the phase velocities for two separate lines using L1-10 and L5-10 data (Figures 6 and 7). Since the accelerometer data were installed oriented in the source coordinate system, we did not have to rotate the waveform data. The rotational component DJZ is compared to CNT. We multiplied the waveform data with the appropriate instrument gain correction and then searched for the best scaling factor (-2*c*) using Equation 3 to match the accelerometer and rotational rate data on all 3 components and for each of the 3 SPE events simultaneously. Horizontal apparent velocities range between 450 and 1125 meters/sec (shear-wave) for L5-10 and L1-10 respectively. The values are consistent with values estimated from surveys and also consistent with different geologies (L1-10 site on weathered Granite is faster).

Figure 8 shows the location of 3 earthquakes within 123 km epicenter distance of the SPE site that occurred around the time of SPE-3 between June and September 2012. The closest of the 3 events on 15-JUN-2012 was a Ml 3.3 was recorded with the highest signal to noise within the 1-10 Hz band (Figure 9). The other two farther earthquakes only had signal above 10 Hz (Figure 11). Figure 9 shows the comparison of the acceleration and rotational motions at station L3-10. The entire waveforms for all 3Cs are completely in phase and the amplitude scaling corresponds to a horizontal phase velocity of 5.4 km/sec with the waveforms rotated to back-azimuth of 271º. Large rotational motions were recorded on all 3C associated with the S-wave phase and small emergent amplitudes for the P-waves and P-coda.

We performed beamforming using only the CNT and DJZ components (Figure 10). The misfit function included a combined sum of the cross-correlation coefficient and amplitude variance reduction scores. We obtained a best fitting wave propagation direction of 271º and horizontal phase velocity of 5.4 km/sec by rotating the acceleration horizontals in 1º increments and scaling the amplitudes in 0.1 km/sec increments. The best-fitting propagation direction is about 20º from the back-azimuth derived from the epicenter-location (251º), however there is a range of 250º to 300º where the fit is as good as the best fitting parameters. The horizontal phase velocity of 5.4 km/sec (range is 5-6 km/sec) is reasonable given the epicenter distance and crustal depth of the earthquake. We do not apply the beamforming to the SPE data since the source-to-receiver distance is only 1 km.

Figure 11 shows the 3C comparison of the two other farther distance earthquakes recorded at station L5-10. The accelerometer and rotational sensors do not have very good sensitivity at lower frequencies and therefore we recorded poor signal-to-noise for smaller and more distance earthquakes. In these cases, we just compared the higher frequencies between 10-20 Hz for the accelerometer and rotational waveforms to show approximate agreement between amplitude envelopes.

Discussions

Rotational ground motions were successfully recorded for the first three SPE chemical explosions at a distance of 1 km. We were able to verify and make sense of the rotational motions using plane-wave assumption in conjunction with co-located accelerometers. Comparisons between P-SV waves, or components CNR-DJT and CNZ-DJR were better than with SH-waves on CNT-DJZ components. We do not expect CNT-DJZ comparisons to be good because transversely polarized S-waves (SH) are not expected from explosion sources. We expect CNT-DJZ to be better because of strong explosion P-and SV-wave radiation from spherical shaped waves from explosion point source. The first arrival within 0.1 sec of the onset at L1-10 CNT-DJZ compared poorly especially for the first cycle which is the P-wave (Figure 6). This indicates either strong departure from plane wave propagation and/or P-SV to SH-wave scattering near the source or generated by the source along joints and fractures identified by other (*e.g.*, *Vorobiev*; *Ezzedine et al.*, this volume). L5-10 comparisons were better for all component pairs (Figure 7). We were fortunate to record a small Ml 3.3 earthquake on 15-June-2012 within 28.7 km of the SPE seismic array and confirm using beamforming that we can estimate reasonable phase velocities and propagation direction using much higher frequency (1-10 Hz) body-waves than in previous studies. Figure 12 illustrates the potential use of rotational ground motions as a discriminant for explosion monitoring. The ratio of peak ground acceleration and peak rotational rate is shown for a range of distances from earthquake and explosion sources. The TAIGER chemical explosions and the Nevada test site nuclear explosion BEXAR are shown to have higher ratios than earthquakes. This ratio is likely similar to P- to S-wave ratios since explosions are likely to generate larger P-wave accelerations but smaller rotational motions due to the lower amplitude S-waves. The reverse is observed with larger shear-waves from earthquakes.

Conclusions

For explosions, rotational and translational motions compare well between the vertical-translational and radial-rotational (CNZ and DJR) components and also for radial-translational and transverse-rotational (CNR and DJT) components. There is a poor comparison between the transverse-translational and vertical-radial (CNT and DJZ) components. Pure isotropic explosions are not expected to radiate transversely polarized P- or S-waves (no SH, only P-SV). Observed CNT and DJZ motions are probably radiated or scattered from fractures or joints near the source. The plane-wave assumption, commonly tested on teleseismic long-period surface-waves, holds true for near-source high-frequency body-waves.

Acknowledgements

SPE would not have been possible without the support of many people from several organizations. The authors wish to express their gratitude to the U.S. Department of Energy, National Nuclear Security Administration, Defense Nuclear Nonproliferation Research and Development and the SPE working group, a multi-institutional and interdisciplinary group of

scientist and engineers. Lawrence Livermore National Laboratory (LLNL) is operated by Lawrence Livermore National Security, LLC, for the U.S. Dept. of Energy, National Nuclear Security Administration under contract DE-AC52-07NA27344. This Is LLNL contribution LLNL-TR-XXXXXX.

References

Aldridge, D. F., and R. E. Abbott (2009). Investigating the point seismic array concept with seismic rotation measurements, Sandia National Laboratory Report SAND2009-0798, Albuquerque, NM, pp 1-58.

Cochard, A., H. Igel, B. Schuberth, W. Suryanto, A. Velikoseltsev, U. Schreiber, J. Wassermann, F. Scherbaum, D. Vollmer (2006). Rotational motions in seismology: Theory, observations, simulation, in Earthquake Source Asymmetry, Structural Media and Rotation Effects, eds. R. Teisseyre, M. Takeo, and E. Majewski, pp. 391-411, Springer, Heidelbeg, Germany, doi: 10.1007/3-540-31337-0_30

Huang, B. (2003). Ground rotational motions of the 1999 Chi-Chi, Taiwan earthquake as inferred from dense array observations, Geophys. Res. Lett., 30(6), 1307, doi: 10.1029/2002GL015157

Igel, H., U. Schreiber, A. Flaws, B. Schuberth, A. Velikoseltsev, and A. Cochard (2005). Rotational motions induced by the M8.1 Tokachi-oki earthquake, September 25, 2003, Geophys. Res. Lett., 32, L08309, doi: 0.1029/2004GL022335.

Igel, H., A. Cochard, J. Wassermann, A. Flaws, U. Schreiber, A. Velikoseltsev, and N. Pham Dinh, Broadband observations of earthquake-induced rotational ground motions, Geophys. J. Int., 168, 182-196, doi: 10.1111/j.1365-246X.2006.03146.x

Langston, C. A., W. H. K. Lee, C. J. Lin, and C. C. Liu (2009). Seismic-wave strain, rotation, and gradiometry for the 4 March 2008 TAIGER explosions, Bull. Seismol. Soc. Am., 99(2B), 1287-1301, doi: 10.1785/0120080200

Lin, C., C. Liu, and W. H. K. Lee (2009). Recording rotational and translational ground motions of two TAIGER explosions in northeastern Taiwan on 4 March 2008, Bull. Seismol. Soc. Am., 99(2B), 1237-1250, doi: 10.1785/0120080176

Lin, C., H. Huang, N. Pham, C Liu, W. Chi, and W. H. K. Lee (2011). Rotational motions for teleseismic surface waves, Geophys. Res. Lett., 38, L15301, doi: 0.1029/2011GL047959.

Liu, C, B. Huang, W. Lee, and C Lin (2009). Observing rotational and translational ground motions at the HGSD station in Taiwan from 2007 to 2008, Bull. Seismol. Soc. Am., 99(2B), 1228-1236, doi: 10.1785/0120080156

Li, Z., and M. van der Bann (2017). Tutorial on rotational seismology and its applications in exploration geophysics, Geophysics, 82(5), W17-W30, doi: 10.1190/GEO2016-0497.

Nigbor, R. L. (1994). Six-degree-of-freedom ground-motion measurement, Bull. Seismol. Soc. of Am., 84(5), 1665-1669.

Nigbor, R. L., J. R. Evans, and C. R. Hutt (2009). Laboratory and field testing of commercial rotational seismometers, Bull. Seismol. Soc. of Am., 99(2B), 1215-1227, doi: 10.1785/0120080247.

Takeo, M. (1998). Ground rotational motions recorded in near-source region of earthquakes, Geophys. Res. Lett., 5(6), 789-792

Takeo, M. (2009). Rotational motions observed during an earthquake swarm in April 1998 offshore Ito, Japan, Bull. Seismol. Soc. of Am., 99(2B), 1457-146, doi: 10.1785/0120080173

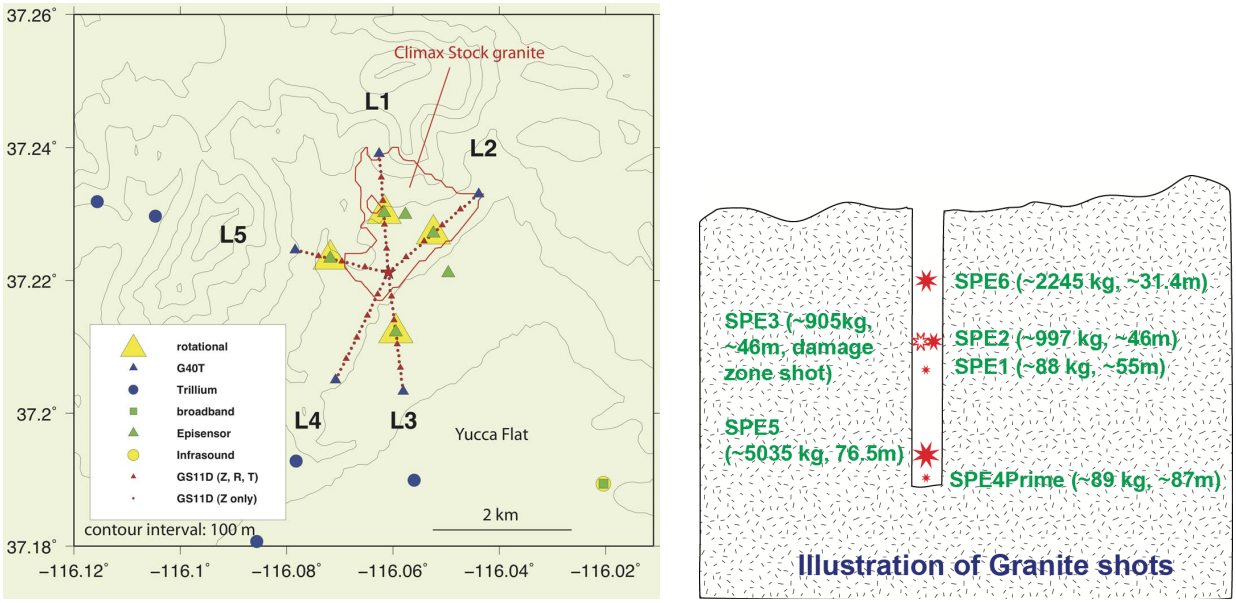

Figure 1. (a) Map of the SPE phase-1 instrument deployment at the NNSS in southern Nevada. (b) Diagram of the SPE phase-1 chemical yield and depth of burial setup in granite

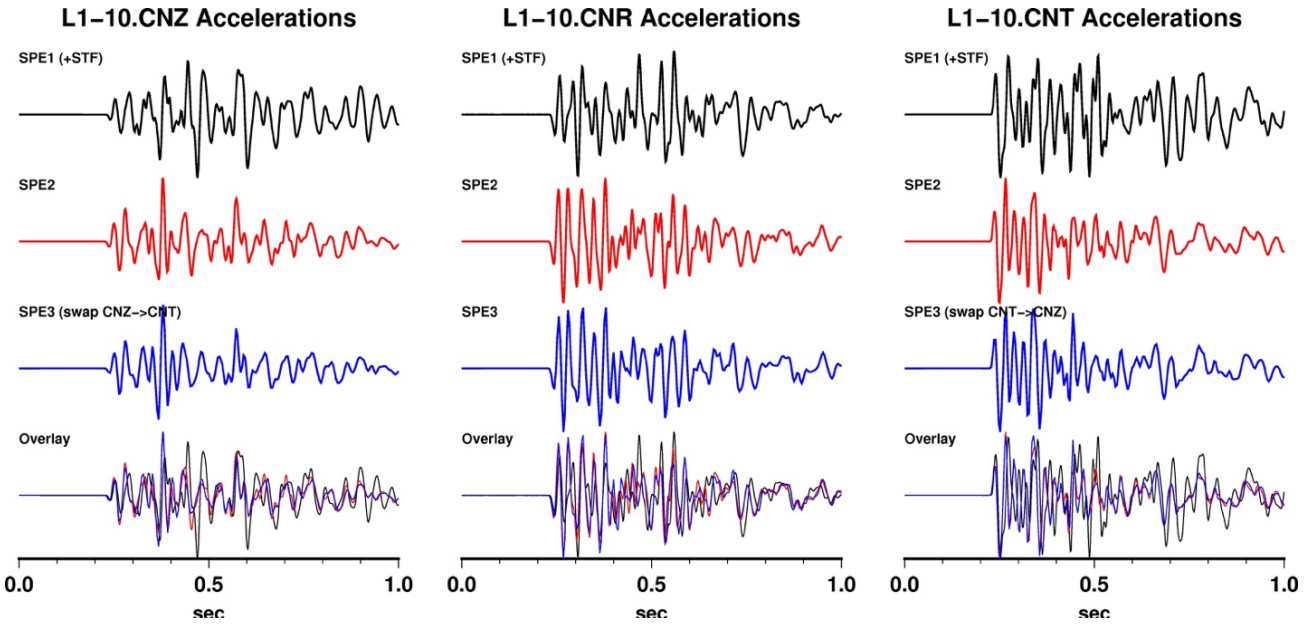

Figure 2. SPE-1, 2, and 3, line 1 station 10 Accelerations

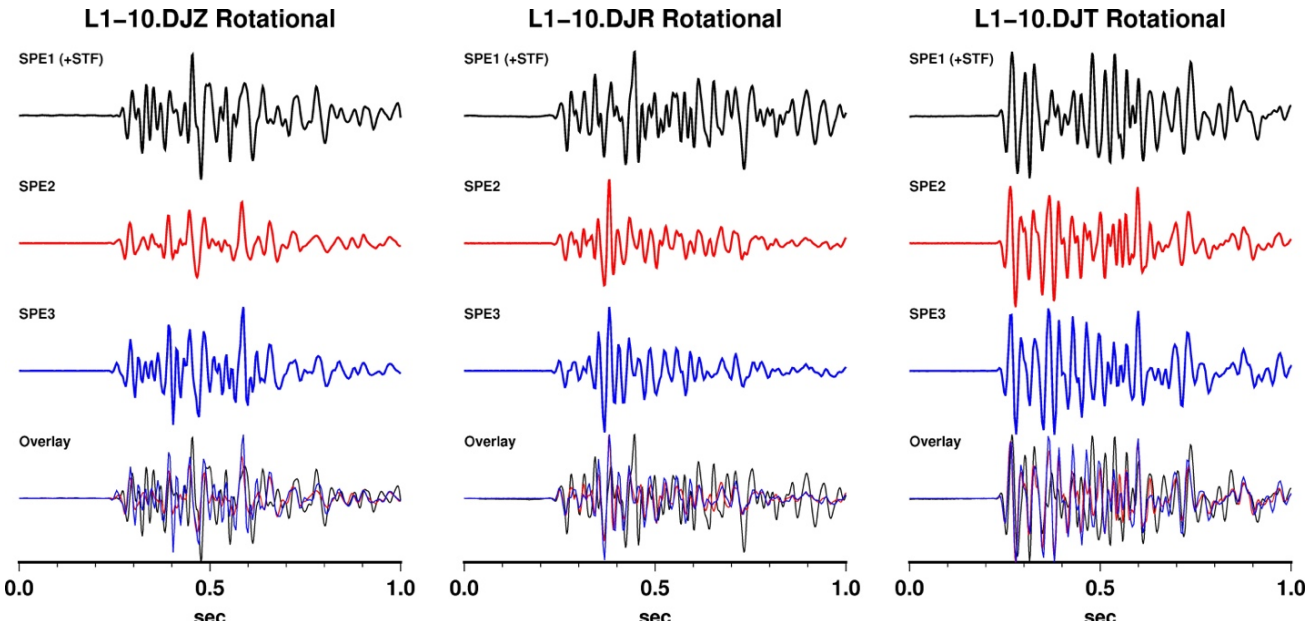

Figure 3. SPE-1, 2, and 3, line 1 station 10 rotations

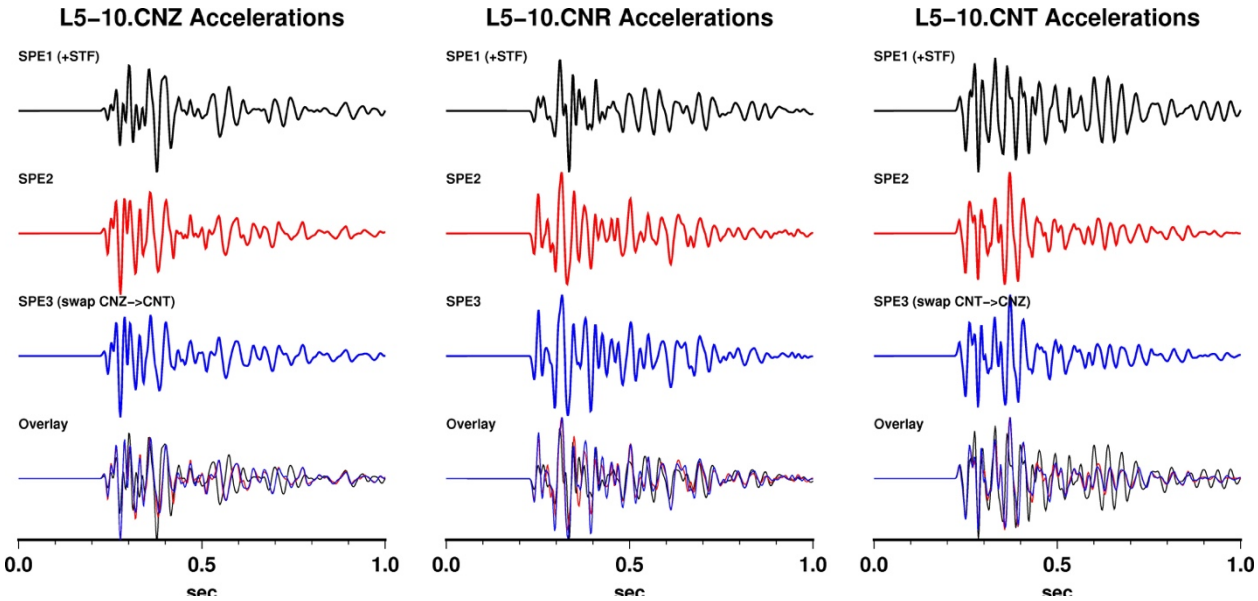

Figure 4. SPE-1, 2, and 3, line 5 station 10 Accelerations

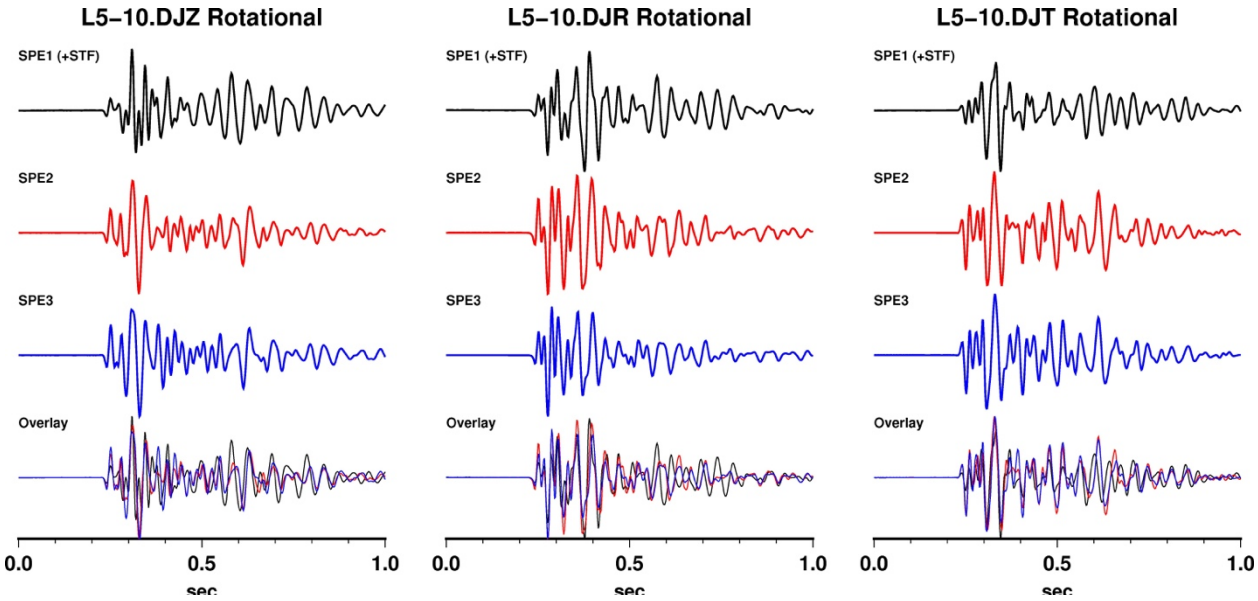

Figure 5. SPE-1, 2, and 3, line 5 station 10 Rotations

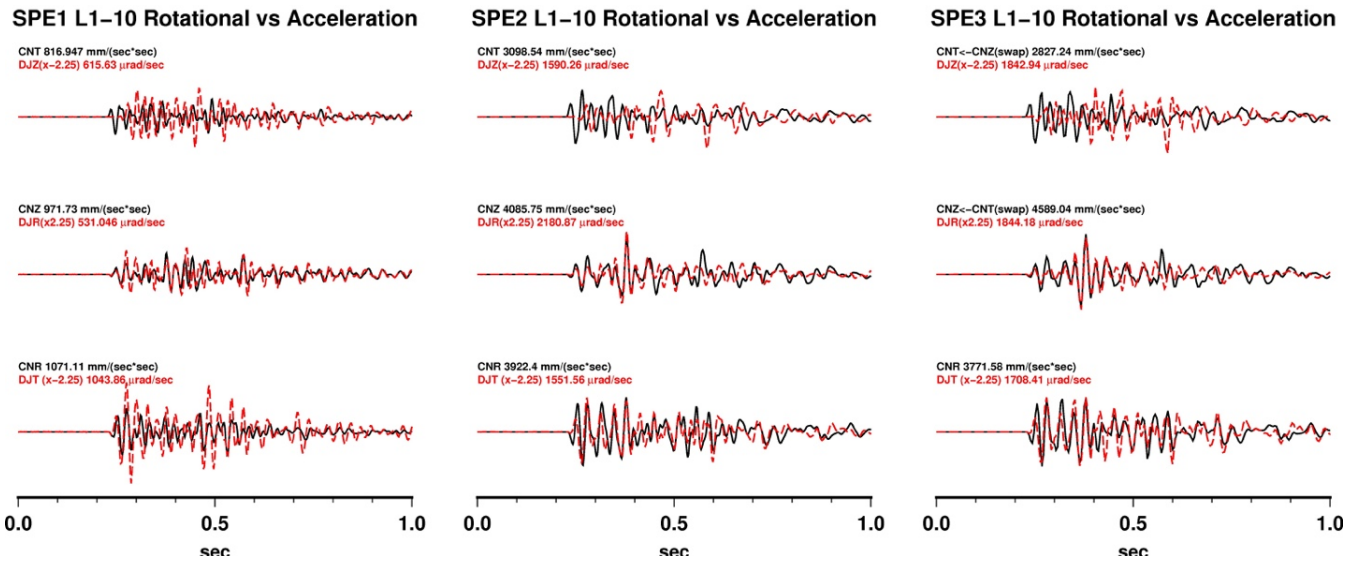

Figure 6. Line 1 station 10 Comparisons (Accelerations and Rotations)

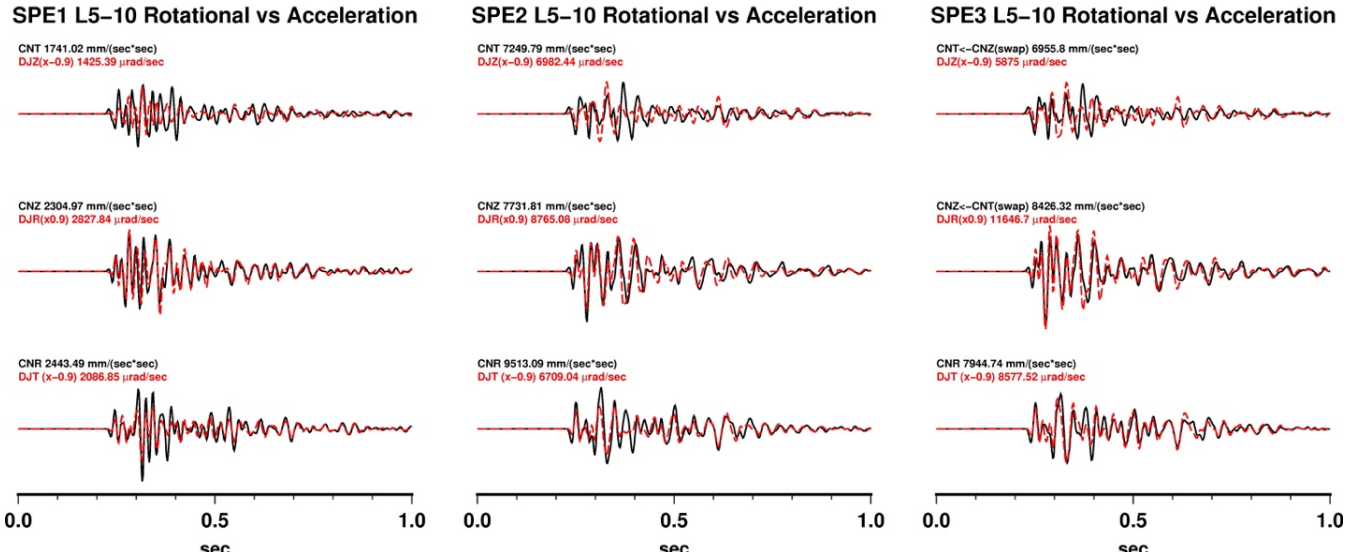

Figure 7. Line 5 station 10 Comparisons (Accelerations and Rotations)

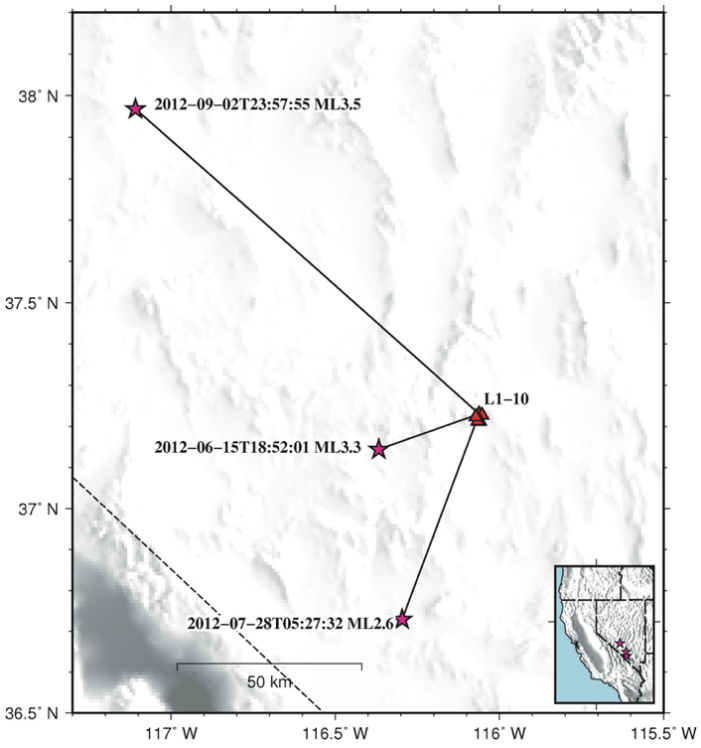

Figure 8. Local Earthquake Map

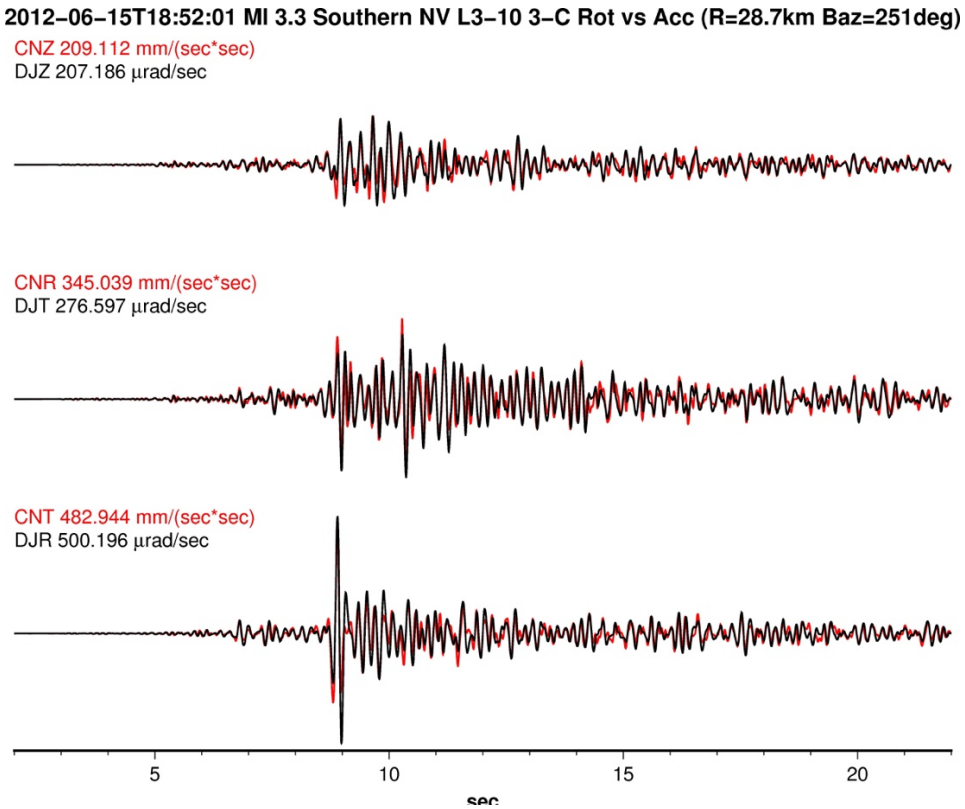

Figure 9. 2012-06-15 Earthquake (ML 3.3)

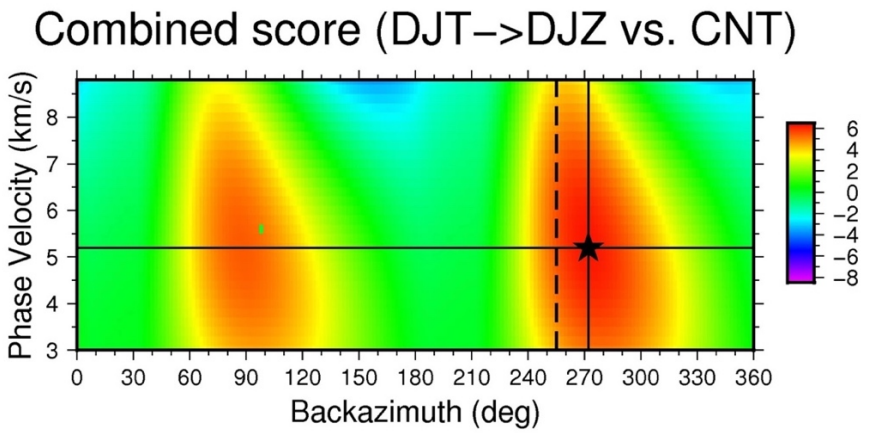

Figure 10. Beamforming using rotational and translational waveforms 2012-06-15 Earthquake (ML 3.3).

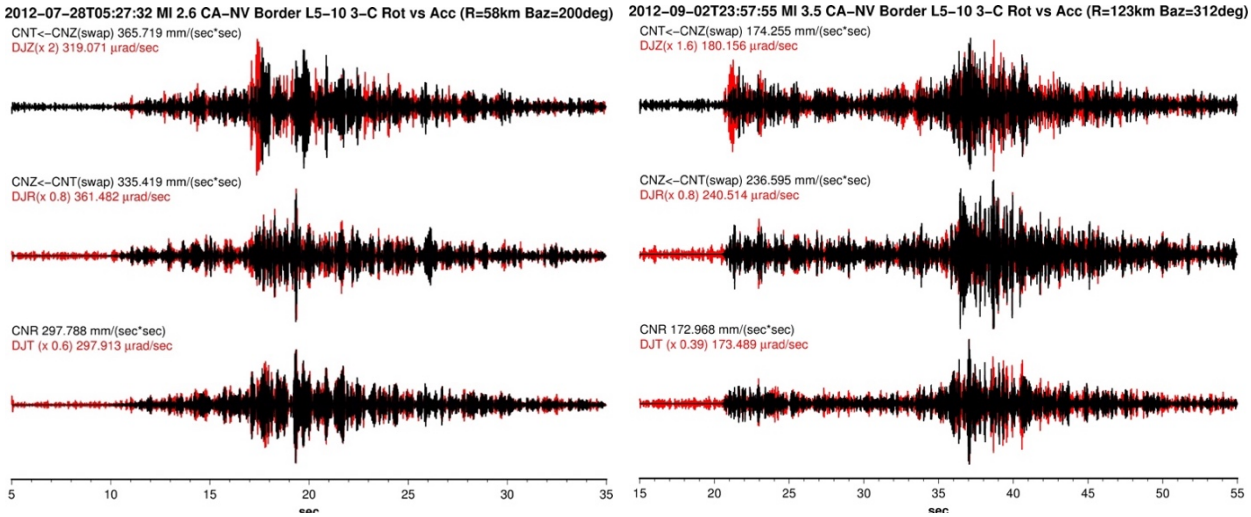

Figure 11. 2012-07-28 Earthquake (ML 2.6), 2012-09-02 Earthquake (ML 3.5)

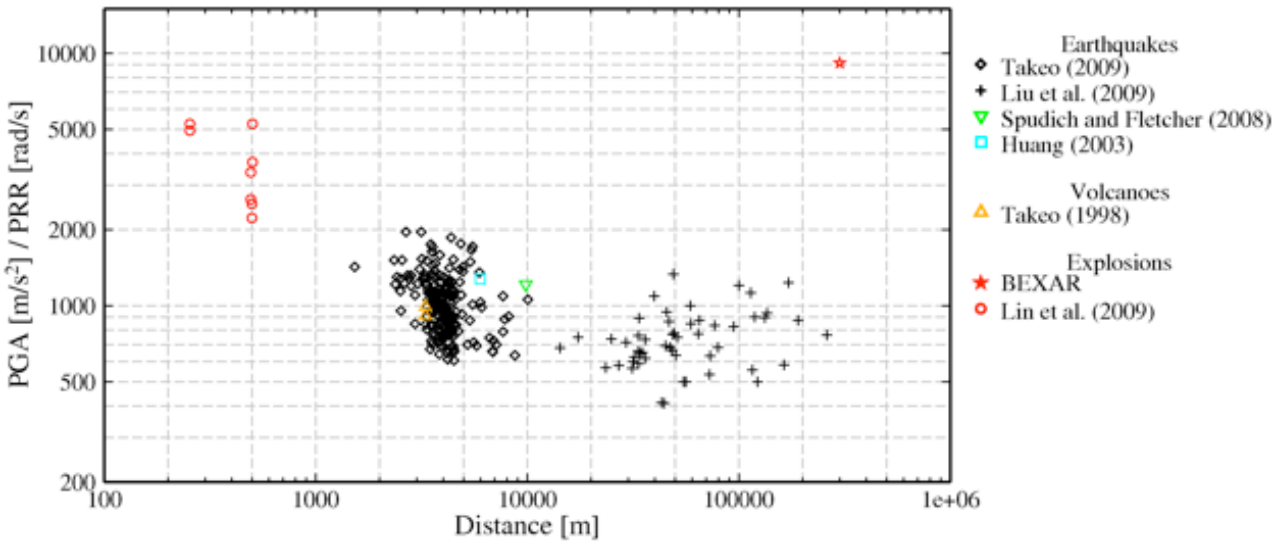

Figure 12. Distance versus the ratio of the Peak Ground Acceleration (PGA) and Peak Rotational Rate (PRR) for earthquakes and explosions.